Talanta 121 (2014) 187–193

Contents lists available at ScienceDirect

Talanta

journal homepage: www.elsevier.com/locate/talanta

Simple and novel electrochemical sensor for the determination of tetracycline based on iron/zinc cations–exchanged montmorillonite catalyst

Tian Gan*, Zhaoxia Shi, Junyong Sun, Yanming Liu

College of Chemistry and Chemical Engineering, Xinyang Normal University, Xinyang 464000, PR China

ARTICLE INFO

Article history:
Received 17 November 2013
Received in revised form
2 January 2014
Accepted 3 January 2014
Available online 10 January 2014

Keywords:
Tetracycline
Electrochemical sensor
Iron
Zinc
Montmorillonite

ABSTRACT

A simple and novel electrochemical sensor for the determination of tetracycline (TC), a kind of antibiotic that may induce residue in the food chain, was developed by the modification of iron/zinc cation–exchanged montmorillonite (Fe/Zn–MMT) catalyst on glassy carbon electrode (GCE). The morphology and the structure of the Fe/Zn–MMT nanomaterial were characterized by scanning electron microscopy and X-ray diffraction, respectively. The results of electrochemical experiments demonstrated that the sensor exhibited excellent electrocatalytic activity to the oxidation of TC in the presence of sodium dodecyl sulfate. The sensor displayed a wide linear range from 0.30 to 52.0 μM and a low detection limit of 0.10 μM by using the derivative differential pulse voltammetry. Moreover, the electrochemical sensor was applied to the detection of TC in feedstuff and meat samples.

1. Introduction

Antibiotic, used in human and animal medicines for controlling microbial infections, as well as incorporated into livestock and poultry feed to increase feed efficiency and improve the growth rate, induce serious residues in the food chain, which can be responsible for toxic effects, allergic reactions in individuals with hypersensitivity [1], and can result in the emergence of harmful bacteria resistant to antibiotics [2]. Therefore, the presence of residues of antimicrobial agents constitutes a potential risk to the human health, and nowadays these antibiotic residues are also recognized as an emerging environmental problem [3,4]. Owing to the low cost and high antimicrobial activity, tetracycline (TC, Scheme 1) is one of the primarily antibiotics groups used for veterinary purposes, for human therapy and in agriculture sector as feed additive [5,6]. Clinical studies of TC have shown that this group of antibiotics have an auxiliary treatment of tumor, inhibit the activity of collagen enzyme and promote bone absorption [7,8]. However, TC resistome is considered to be the largest resistome against an individual class of antibiotics because this resistome was reported to have over 189 tet genes in bacteria [9]. And tetracycline can be deposited in bones and teeth leading to the inhibition of bone growth [10]. This has spurred the development technologies for rapid and accurate detection of TC extensively.

Up until now, many analytical methods have been developed for the detection of TC, such as chromatography [11], fluorescence [12], luminescence [13], and electrochemistry techniques [14–22]. Among various approaches, electrochemical sensors for TC have attracted much attention, owing to their advantages of convenience, operation simplicity, and suitability for real-time detection [23,24]. As a result, electrochemical sensors based on DNA [14], aptamer [15], antibody [16] and molecularly imprinted polymer [17] have been fabricated because of their high selectivity and sensitivity. Their application, however, is limited because of their costliness, easy denaturation and complicated immobilization procedure. Thus, the development of a high sensitivity and good selectivity catalyst for direct TC detection is still highly desirable in this field. Calixto et al. [18] evaluated the determination of TC in natural water samples using graphite–polyurethane composite electrode. A detection limit of 2.80 μM was obtained. Masawat et al. [19] fabricated a disposable screen-printed gold electrode to determine TC residues in food with a detection limit of 0.96 μM. A gold modified microelectrode was developed by Wang et al. [20] and used to direct TC detection with a detection limit of 187 nM. The voltammetric behavior of TC at multi-wall carbon nanotube-ionic liquid film modified glassy carbon elelctrode (GCE) was studied by Guo et al. [21]. The detection limit for TC was estimated to be 30 nM after 150–s accumulation. Otherwise, a low detection limit of 12 nM for the detection of TC based on acetylene black

* Corresponding author. Tel.: +86 376 6390702; fax: +86 376 6390597.
E-mail address: gantsjy@163.com (T. Gan).

0039-9140/$ - see front matter © 2014 Elsevier B.V. All rights reserved.
http://dx.doi.org/10.1016/j.talanta.2014.01.002

electrode in the presence of sodium dodecyl sulfate (SDS) was reported by Dang et al. [22], which showed the sensitizing effect of SDS.

Montmorillonite (MMT) science and its application have received increasingly wide attention in the areas of physics, chemistry, environmental and materials areas because of its abundance, cheapness, environmental compatibility, high surface areas, surface reactivity and cation exchange capacity [25]. The layers of MMT consist of two tetrahedral silica sheets sandwiching one octahedral alumina sheet [26]. And the negative surface charges between the clay platelets are balanced by Ca^{2+}, Mg^{2+}, or Na^{+} cations, which can be easily exchanged with other metal cations which could lead to the enhancement of its dispersion in the continuous phase, the increase of surface area, and the exfoliation or intercalation behavior of MMT [27], which in turn improves nanocomposite performance.

In this work, Fe and Zn mixed nanoparticles were intercalated into MMT nanolayers through cations-exchange technique to increase the catalytic ability of MMT considerably. And a simple, rapid and convenient electrochemical sensor for the detection of TC was fabricated using Fe/Zn–MMT as sensing film. The electrochemical behaviors of TC were studied in the presence of SDS. It was found that Fe/Zn–MMT modified GCE greatly increased the oxidation signal of TC, compared with the bare GCE. Fe/Zn–MMT exhibited high accumulation efficiency and remarkably enhanced the surface concentration of TC due to the high surface area and swelling layered structure. As a result, a simple and novel monitoring system was developed for TC. Moreover, the newly developed sensor owns promising application for the determination of TC in real samples.

2. Experimental

2.1. Reagents

All chemicals were of analytical grade and used directly. TC (Sigma) was dissolved into 0.1 M HCl to prepare 1.0 mg mL^{-1} standard solution, and stored at 4 °C. Anhydrous iron nitrate ($FeNO_3$), zinc nitrate hexahydrate ($ZnNO_3 \cdot 6H_2O$), SDS, cetyltrimethylammonium bromide (CTAB) and sodium dodecyl benzene sulfonate (SDBS) were purchased from Sinopharm Chemical Reagent Company (Shanghai, China). Nano-sodium MMT (~25 nm) was obtained from the Fenghong Clay Chemicals Co., Ltd. (Zhejiang, China). The content of MMT was 96–98%, and the apparent density and diameter thickness ratio of the material were 0.25–0.35 g cm^{-3} and 200, respectively. Doubly distilled water (the resistivity of which is 1.3×10^6 Ω cm) was used throughout.

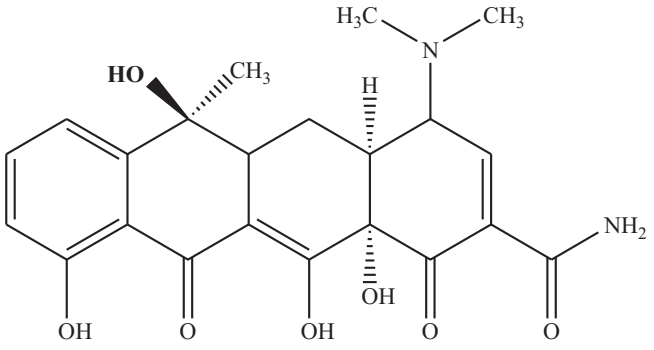

Scheme 1. The chemical structure of tetracycline.

2.2. Apparatus

Electrochemical measurements were performed on a CHI 660E electrochemical workstation. A conventional three-electrode system, consisting of a Fe/Zn–MMT film modified GCE, a saturated calomel reference electrode (SCE) and a platinum wire auxiliary electrode, was employed. Scanning electron microscopy (SEM) characterization was conducted with a Hitachi S-4800 microscopy (Japan). X–ray diffraction (XRD) was recorded on a Rigaku D/max-2500, using Ni filtered Cu K_α radiation ($\lambda = 0.154$ nm) as a source (current intensity, 100 mA; voltage, 40 kV) and a Xcelerator detector.

2.3. Synthesis of Fe and Zn modified MMT

The Fe and Zn modified MMT (Fe/Zn–MMT) was prepared according to Jha et al. [28] with some modification. In a typical preparation, 40 mL of 0.2 M-$FeNO_3$ and $ZnNO_3 \cdot 6H_2O$ mixed aqueous solution was slowly added into 2.5 g nano-MMT, and stirred for 4 h at room temperature. After filtering, washing with abundant water and being dried in a vacuum oven at 373 K for 2 h, the product was grinded to powder and then calcined in a furnace at 573 K for 3 h with a heating rate of 2 °C/min, which was denoted as Fe/Zn–MMT. The schematic representation for the preparation of Fe/Zn–MMT was shown in Scheme 2.

2.4. Preparation of the TC sensor

A GCE (diameter of 3 mm) was firstly polished with 0.05 μm alumina slurry on silk, and then washed with ethanol/water (1:1, V/V) and water in an ultrasonic bath, each for 1 min. The suspension of Fe/Zn–MMT was prepared by acutely stirring 20.0 mg of Fe/Zn–MMT powder in 10.0 mL water for 24 h. For fabricating the TC sensor, 10.0 μL of the obtained Fe/Zn–MMT colloid solution was coated onto the surface of GCE and allowed to dry under an infrared lamp in the air, which was denoted as Fe/Zn–MMT/GCE, too.

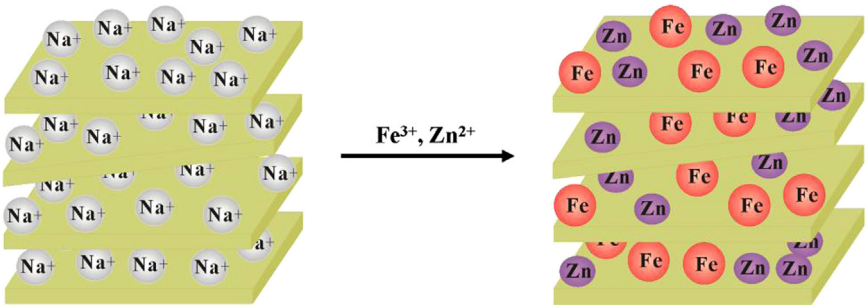

Scheme 2. Schematic representation of the cation exchange reaction that leads to Fe/Zn–MMT.

2.5. Sample pretreatment

2.5.1. Chicken feed sample

Chicken feed sample spiked with target TC, was prepared by adding the stock solution of TC with spiked level of 0.2 mg g^{-1} to the feed sample, and then the sample was shaken for 2 min by a Model XK96-B shaker (Shanghai, China) to mix completely. It was subsequently evaporated to dryness in air and stored at 4 °C in dark. 0.1 g of this spiked chicken feed sample was weighed accurately and mixed with 5.0 mL aliquot of ethyl acetate in a 10 mL centrifuge tube. Then, the sample was treated in an ultrasonic bath for 20 min and centrifuged for 10 min at 4000 rpm. The upper ethyl acetate layer (3.2 mL) was transferred into a 10 mL centrifuge tube, which was evaporated to dryness at room temperature. Finally, the obtained dried deposit was dissolved with 500 μL methanol and diluted to 5.0 mL with water.

2.5.2. Fish, chicken and shrimp samples

A weighed aliquot of fish (6 g) was homogenized in 3.0 mL of 0.1 mol L^{-1} EDTA and 2.0 mL of pH 4.0 McIlvaine buffer with the use of a model HY-4 homogenizer (Shanghai Instrumental Manufacturing, China) at 4000 rpm for 15 min. Such a sample was shaken for 5 min with 3 mL-acetonitrile. It was then, centrifuged at 4000 rpm for 10 min, decanted into a clean polypropylene tube. Furthermore, the fish residue was extracted with another 3.0 mL aliquot of acetonitrile. The two extracts were then combined and evaporated to dryness with nitrogen. Dried extract was reconstituted in 200 μL methanol, which was centrifuged under the same conditions as before and stored at 4 °C in the dark. The chicken and shrimp samples were pretreated using the same procedures.

2.6. Experimental procedure

Unless otherwise stated, a 0.1 M H_2SO_4 solution was used as the supporting electrolyte for the determination of TC. The differential pulse voltammograms were recorded from 0.8 to 1.15 V after 3 min of accumulation in the presence of SDS, and the voltammetric curves were treated with the semi-derivative technique on a CHI 660E electrochemical workstation.

3. Results and discussion

3.1. Characterization of Fe/Zn–MMT nanocomposite

The surface morphology of the Fe/Zn–MMT film modified GCE was characterized by SEM (Fig. 1). Compared with the rather smooth surface of GCE (a), lots of uniform and compact film comprising folded MMT layers and many nanopores is observed at Fe/Zn–MMT/GCE (b), which is covered by the uniform Fe and Zn nanoparticles as indicated in the inset of Fig. 1b. So the effective surface area of the electrode can be extended to a large extent. Furthermore, the edge of the Fe/Zn–MMT layers is kinkled, proving the ultra-thin nanosheets of this nanohybrid, which may provide substantial channels for electrons transfer.

It is well known that MMT is a swelling clay that contains water of hydration. Since the hydration state of MMT is expected to be reflected by the size of its interlayer space, the effect of iron and zinc cations sorption on the basal space (d_{001}) of MMT was studied using XRD [29]. The XRD patterns of the MMT and Fe/Zn–MMT are presented in Fig. 2. The d_{001}-values for the basal reflection at $2\theta = 6.5^\circ$ in Fe^{3+} and Zn^{2+}–exchanged MMT sample was almost similar to the parent MMT (13.45 Å), indicating that the interlayer separation was not affected by the Fe^{3+} and Zn^{2+} exchange process [28]. However, the intensity of the d_{001} diffraction for the Fe/Zn–MMT was some slightly decreased with the exchange of mixed metal cations, indicating an insignificant decrease of the crystallinity of the MMT [30].

3.2. Electrochemical property of Fe/Zn–MMT film modified GCE

Electrochemical impedance spectrometry (EIS) is one of the most effective tools for exploring the interface property of chemically modified electrodes. Fig. 3 shows the EIS results of 5 mM $K_3Fe(CN)_6$ in 0.1 M KCl at bare GCE (a) and Fe/Zn–MMT/GCE (b). The EIS spectra include a semicircular part at high frequencies and a linear part at low frequencies, corresponding to the electron transfer process and the diffusion process, respectively. The semicircle of Fe/Zn–MMT/GCE with a much smaller diameter indicates a faster electron transfer rate between $K_3Fe(CN)_6$ and the electrode surface compared with bare GCE, probably due to the Fe/Zn mixed metals that endows strong catalytic effect to MMT.

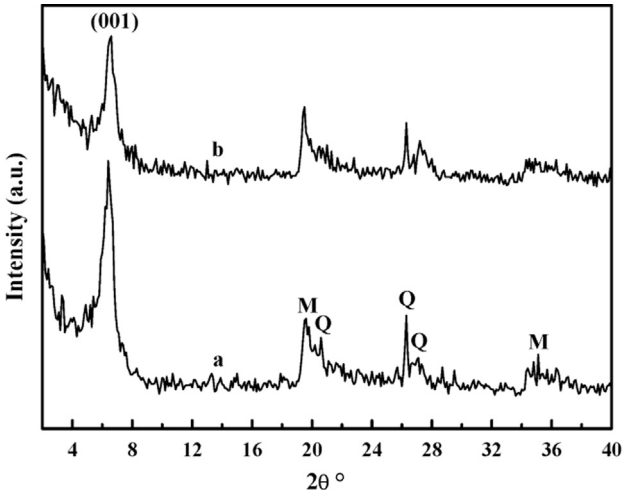

Fig. 2. XRD patterns of MMT (a) and Fe/Zn–MMT (b).

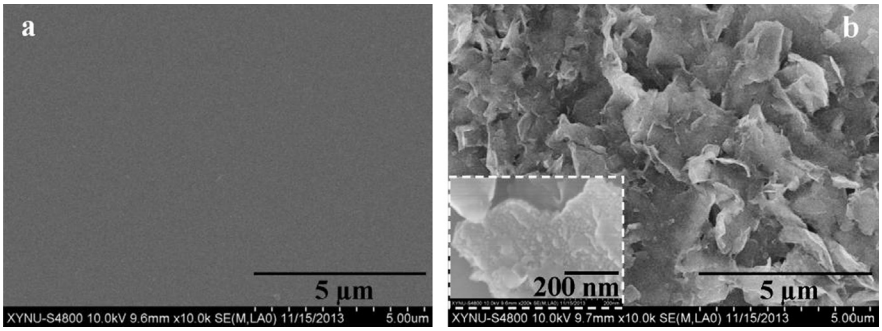

Fig. 1. SEM images of bare GCE (a) and Fe/Zn–MMT/GCE (b). Inset of (b) shows the high magnification morphology of Fe/Zn–MMT film.

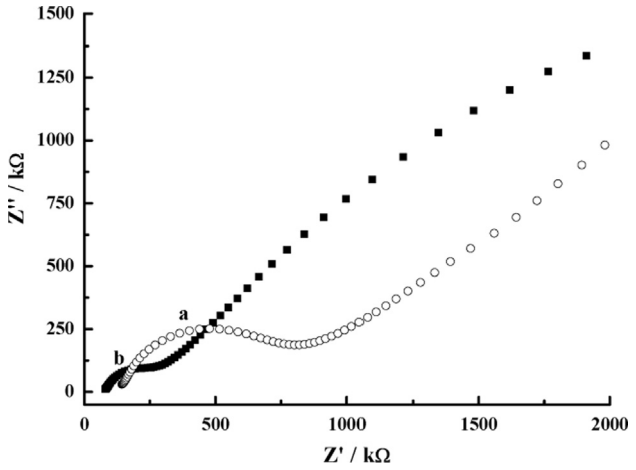

Fig. 3. Nyquist diagram (Z'' vs. Z') for the EIS measurements in the presence of 10 mM $K_3Fe(CN)_6$ in 0.1 M KCl at bare GCE (a) and Fe/Zn–MMT/GCE (b).

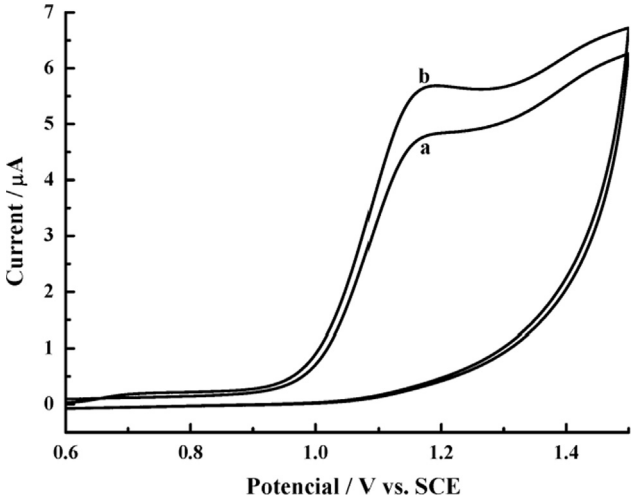

Fig. 4. Cyclic voltammograms of 52 μM TC at bare GCE (a) and Fe/Zn–MMT/GCE (b) in 0.1 M H_2SO_4 in the presence of 0.7 mM SDS. Scan rate = 5 mV s^{-1}.

3.3. Electrochemical oxidation of TC at the sensor

The electrochemical behaviors of TC at the bare GCE and this sensor were investigated by cyclic voltammetry (CV). Fig. 4 shows the cyclic voltammograms of 52 μM TC in 0.1 M H_2SO_4 in the presence of 0.7 mM SDS. During the anodic potential sweep from 0.60 to 1.50 V, one oxidation peak is observed at about 1.17 V on the bare GCE (a) and the Fe/Zn–MMT/GCE (b), respectively. On the following reverse sweep, no corresponding reduction peak is observed on both electrodes, suggesting that the electrode processes of TC on the bare GCE and the sensor are totally irreversible. From the comparison of curves (a) and (b), it is very clear that the oxidation peak current of TC increased at the modified electrode, which demonstrates that the Fe/Zn–MMT modified GCE holds the properties that are favorable for the oxidation of TC. The Fe/Zn–MMT/GCE has large surface area, i.e., a larger electrochemical reaction interface compared with the bare GCE, which undoubtedly can adsorb more TC onto the surface of the electrode, and therefore shows better performance towards the oxidation of TC.

The oxidation responses of TC on the surface of bare GCE, MMT/GCE, Zn–MMT/GCE, Fe–MMT/GCE and Fe/Zn–MMT/GCE were compared using differential pulse voltammetry (DPV) in the presence of 0.7 mM SDS through semi-derivative processing. As shown in Fig. 5, curve a, an oxidation peak at 1.03 V is observed on GCE surface, and the peak current is relatively low (1.52 μA). The

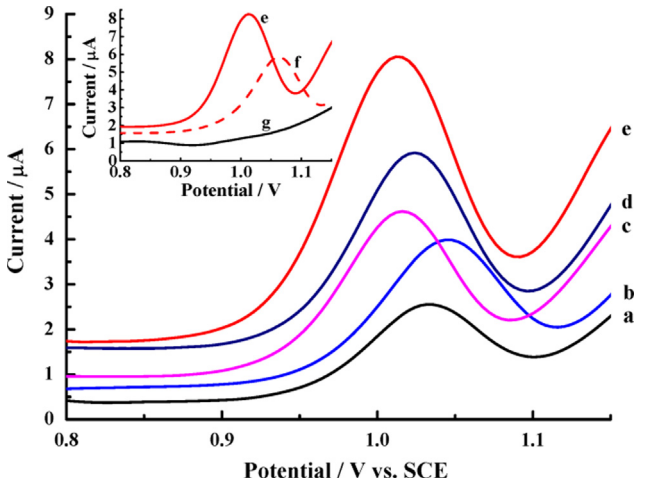

Fig. 5. Semi-derivative DPV graphs of bare GCE (a), MMT/GCE (b), Zn–MMT/GCE (c), Fe–MMT/GCE (d) and Fe/Zn–MMT/GCE (e) in 0.1 M H_2SO_4 containing 21.0 μM TC and 0.7 mM SDS. Inset: semi-derivative DPV behaviors of 21.0 μM TC at Fe/Zn–MMT/GCE in 0.1 mol/L H_2SO_4 with (e) and without 0.7 mM SDS (f). Curve g corresponds to semi-derivative DP voltammogram of Fe/Zn–MMT/GCE in blank solution in the presence of 0.7 mM SDS. Accumulation time = 180 s.

weak oxidation signal indicates that the oxidation activity of TC is poor on bare GCE surface. The oxidation peak of TC is apparently enhanced by the modification of MMT on GCE surface (I_p = 2.40 μA, Fig. 5, curve b), indicating the bigger surface area brought by the layered MMT. At Zn–MMT/GCE (Fig. 5, curve c) and Fe–MMT/GCE (Fig. 5, curve d), the oxidation peak current of TC is further improved to 2.85 and 3.53 μA, respectively. This is caused by the immobilization of metal nanoparticles on MMT surface that can greatly improve the surface area of GCE (see Fig. 1). Furthermore, significantly negative shift of the oxidation potential of TC is observed at Zn–MMT/GCE and Fe–MMT/GCE compared to bare GCE. This demonstrates the plenty of electroactive sites for the TC oxidation provided by Zn and Fe nanoparticles. In addition, the oxidation wave is increased by 2.4-fold on the surface of Fe/Zn–MMT/GCE (Fig. 5, curve e). The notable peak current enlargement shows that Fe/Zn bimetal modified MMT nanocomposite exhibits strong synergistic enhancement effect toward the oxidation of TC.

The influence of SDS on the voltammetric response of TC was also studied (inset of Fig. 5). The oxidation peak current of TC is 3.17 μA at 1.06 V in the absence of SDS on Fe/Zn–MMT/GCE (curve f). However, the peak current increases to 5.14 μA at 1.01 V on the same sensor in the presence of 0.7 mM SDS. Evidently, the SDS facilitates the anodic reaction of TC, which may be caused by its micellar or ion pairing effects [31]. Furthermore, the sensor does not show any oxidation response in the absence of TC at the same condition as curve e (curve g), indicating the attribution of the oxidation peak to TC.

3.4. Influence of scan rate on the oxidation of TC at the sensor

In order to investigate the electrode process of TC at this sensor, the electrochemical responses of 52 μM TC were studied using CV at relative low scan rate in 0.1 M H_2SO_4 in the presence of 0.7 mM SDS. It was found that the oxidation peak current (I_p, μA) of TC increased linearly in the scanning rate (ν, mV s^{-1}) range of 3–20 mV s^{-1} (Fig. 6). As inset A of Fig. 6 shows, there is good linear relationship between I_p and $\nu^{1/2}$, and the linear regression equation is $I_p = -0.389 + 2.663\nu^{1/2}$ ($r^2 = 0.995$), indicating that the oxidation of TC on this sensor is a diffusion-controlled process at low scan rate. Meanwhile, the oxidation peak potential (E_p, V) positively shifted with the scan rate (ν, mV s^{-1}) (inset B of Fig. 6), and the relationship between them is in accordance with the

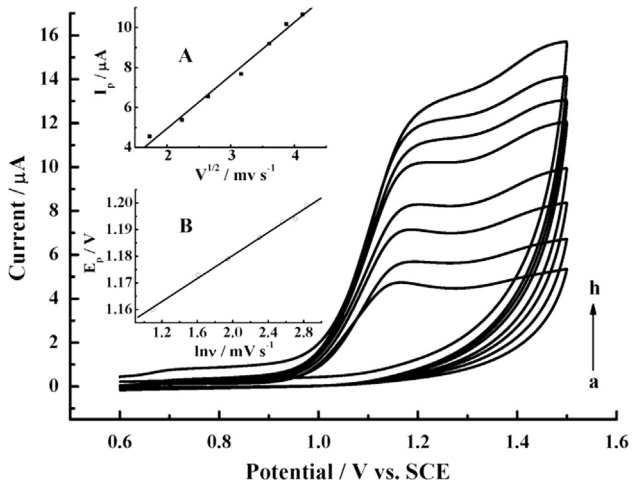

Fig. 6. Cyclic voltammograms of 52.0 μM TC in 0.1 M H_2SO_4 at the sensor with different scan rates including 3 (a), 5 (b), 7 (c), 10 (d), 13 (e), 15 (f), 17 (g) and 20 (h) mV s^{-1}. Inset: linear relationship of I_p vs. $\nu^{1/2}$ (A) and E_p vs. ln ν (B).

following equation [32]:

$$E_p = E^{0'} + \frac{RT}{\alpha nF}\left[0.780 + \ln\frac{D_R{}^{1/2}}{k^0} + \ln\left(\frac{\alpha nF\nu}{RT}\right)^{1/2}\right]$$

$$= K + \frac{RT}{2\alpha nF}\ln\nu \quad (1)$$

where $E^{0'}$ is the formal potential, D_R is the diffusion coefficient of TC, k^0 is the standard heterogeneous rate constant, α is the transfer coefficient of the oxidation of TC. Other symbols have their usual significance. According to Eq. (1), the plot of E_p vs. ln ν has a good linear relationship, from which the value of αn can be calculated to be 0.59 from the slope (i.e., 0.0216). Generally, α in the totally irreversible electrode process is assumed to be 0.5, consequently, one electron is involved in the oxidation of TC.

3.5. The optimization of experimental conditions

3.5.1. Optimization of the medium system

To find the optimum experimental conditions, several supporting electrolytes were tested including 0.1 M HCl, 0.1 M H_2SO_4, 0.1 M $HClO_4$, 0.1 M HNO_3 and a number of buffers including McIlvaine buffer (pH 2.2–8.0), Britton–Robinson buffer (pH 1.81–11.58), boric acid–borax buffer (pH 7.4–9.0), acetate buffer (pH 2.6–5.0), glycine–sodium hydroxide buffer (pH 8.6–10.6), carbonate buffer (pH 8.77–10.83) and phosphate buffer (pH 5.8–8.0). It was found that the best defined peak wave and the highest sensitivity for the TC can be obtained in 0.1 M H_2SO_4 solution.

The influence of surfactant type on the oxidation peak current of 21.0 μM TC was explored by semi-derivative DPV. The peak current is less than 3.0 μA in the presence of cationic surfactants (i.e., CTAB). However, the peak current is higher in the presence of anionic surfactants like SDS and SDBS. And the voltammetric response is the highest in the presence of SDS, which is attributed to the different surface activity of these surfactants [33]. Additionally, the effect of the concentration of SDS in electrolyte on the oxidation signal of TC was also investigated. It is found that the biggest peak current of 21.0 μM TC appears when the concentration of SDS is fixed to 0.7 mM, which may because this concentration can form suitable micelle in the solution and then transfer the TC molecules to electrode surface.

3.5.2. Optimizing of the accumulation conditions

In electrochemical determination, accumulation is an effective and simple way to improve the determining sensitivity. In this work, the effects of accumulation potential and time on the oxidation peak current of TC were investigated. In order to evaluate the influence of accumulation potential on the determination of TC, the oxidation peak current of 21 μM TC after 180–s accumulation under different accumulation potentials as well as under open-circuit was measured by semi-derivative DPV. It is found that the oxidation peak current changes evidently as changing accumulation potential from 0.4 to 0.8 V, and the oxidation of TC shows the biggest peak current at the accumulation potential of 0.6 V, which is applied in the following accumulation step.

Subsequently, the influence of accumulation time on the oxidation peak current of 21 μM TC was investigated. The oxidation peak current is very low without accumulation. When gradually increasing accumulation time from 0 to 180 s, the oxidation peak current almost linearly increases. As improving the accumulation time, more and more TC accumulates at the sensor surface, so the oxidation peak current greatly increases. However, the oxidation peak current almost keeps a constant when the accumulation time is longer than 180 s, suggesting that the amount of TC at the sensor surface tends to saturation. Considering both sensitivity and working efficiency, an accumulation time of 180 s was selected.

3.6. Analytical properties

3.6.1. Anti-interference

The anti-interference ability of the proposed sensor is examined and the experimental results are shown in Table 1. Some cations and organic compounds that may exist in real food samples were selected here. It can be seen that the addition of some inorganic ions such as Na^+, K^+, Mg^{2+}, Zn^{2+}, Al^{3+}, Cu^{2+} and Ca^{2+} do not interfere with TC detection. Some organic substances such as 1000-fold glucose, sucrose and glycine; 500-fold citric acid and 100-fold ascorbic acid also do not interfere the determination of 21.0 μM TC (the peak current change is below 7%). Additionally, some antibiotic like oxytetracycline, aureomycin, chloramphenicol and rifampicin have no influence on the detection of TC at the same concentration as TC.

3.6.2. Reproducibility

The successive measurements using one sensor were examined, and unfortunately the oxidation peak current of TC decreased continuously. The strong surface sorption and fouling were the main reason. Thus, the sensor was used for single measurement, and the reproducibility between multiple sensors was evaluated by parallel determination of the oxidation peak current of 21.0 μM TC. The relative standard deviation (RSD) is 5.2% for 10 sensors,

Table 1
Influences of possible interferents on the anodic peak current of 21.0 μM TC.

Interferents	Tolerance level (M)	Signal change (%)
K^+	4.20×10^{-2}	−2.3
Na^+	3.15×10^{-2}	6.7
Mg^{2+}, Zn^{2+}, Al^{3+}	1.05×10^{-2}	−4.5, −3.2, −7.3
Cu^{2+}, Ca^{2+}	2.10×10^{-3}	−3.2, 6.4
Glucose, sucrose, glycine	2.10×10^{-2}	−3.4, 2.2, 4.0
Citric acid	1.05×10^{-2}	−5.1
Ascorbic acid	2.10×10^{-3}	6.3
Oxytetracycline, aureomycin, chloramphenicol, rifampicin	2.10×10^{-5}	5.0, 4.9, −5.3, 6.5

Table 2
Comparison of the analytical performance of this sensor with previous work.

Modified electrode	Linear range (μM)	LOD (nM)	Reference
Graphite–polyurethane composite electrode	4.00–40	2800	[18]
Screen-printed gold electrode	1–500	960	[19]
Gold modified microelectrode	2.08–20.8	187	[20]
	20.8–208		
Multi-wall carbon nanotube-ionic liquid modified GCE	0.11–22	30	[21]
Acetylene black modified carbon paste electrode	0.12–60	12	[22]
Fe/Zn–MMT modified GCE	0.104–52	10.7	This sensor

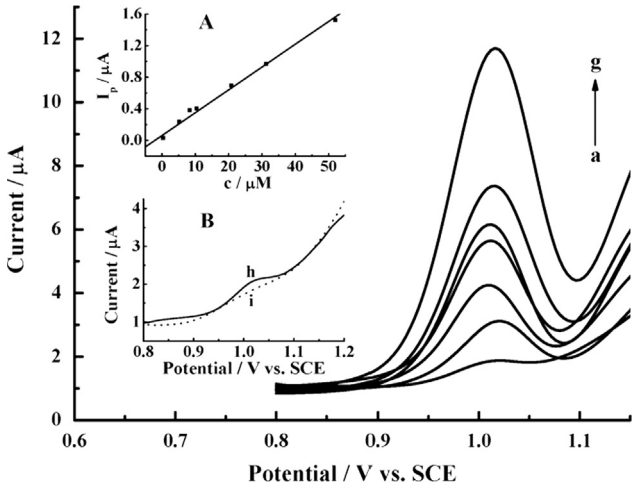

Fig. 7. Semi-derivative DPV graphs of (a) 0.30, (b) 5.0, (c) 8.0, (d) 10.5, (e) 20.5, (f) 31.0 and (g) 52.0 μM TC in 0.1M H_2SO_4 solution and 0.7 mM SDS at the sensor. Inset A: linear relationship between I_p and the concentration of TC. Inset B: semi-derivative DPV behaviors of this sensor in 0.10 μM TC (h) and blank solution (i). Other conditions are as Fig. 5.

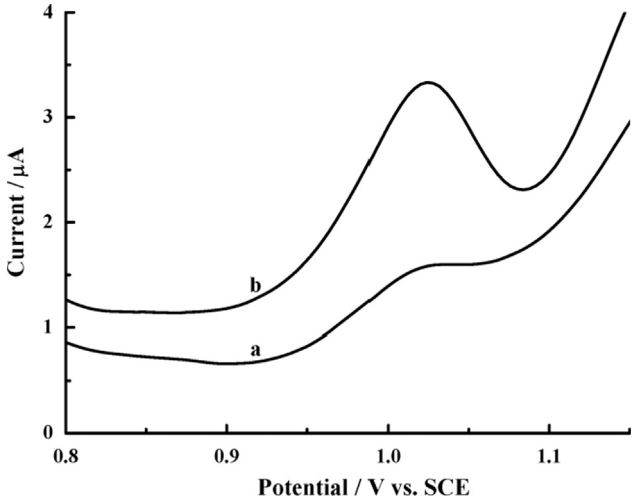

Fig. 8. Semi-derivative DPV curves of chicken feed sample (a) and spiked chicken feed sample (b) on the sensor. Other conditions are as Fig. 5.

indicative of excellent fabrication reproducibility and detection precision.

3.6.3. Linear range and limit of detection

Under the optimized conditions, the linear range and limit of detection were investigated using semi-derivative DPV technique in 0.1 M H_2SO_4 and 0.7 mM SDS. Fig. 7 shows that the oxidation peak current (I_p, μA) of TC changes linear with its concentration

Table 3
Detection and recovery of TC in chicken feed, fish, chicken and shrimp samples.

Sample	Detection		Spiked (M)	Recovery test	
	The sensor (M)	RSD (%)		Found (M)	Recovery (%)
Chicken feed	4.90×10^{-6}	2.6	4.32×10^{-6}	4.20×10^{-6}	97.2
Fish			8.07×10^{-6}	8.31×10^{-6}	103
Chicken	2.36×10^{-5}	5.0	1.04×10^{-4}	1.03×10^{-6}	99.0
Shrimp			2.08×10^{-4}	2.03×10^{-4}	97.6

(c, μM) in the range of 0.30–52 μM (curves a∼g), obeying the following equation: $I_p = 0.062 + 0.029c$ (Inset A of Fig. 7). And the limit of detection (LOD) was obtained as 0.10 μM through decreasing the concentration of TC gradually (curve h in inset B of Fig. 7) and 10.7 nM through $S/N = 3$. The comparison of the analytical performance of this sensor with previous work is shown in Table 2. It can be seen that the limit of detection in our work is the lowest compared with other techniques that are based on the direct electrochemical signal of TC.

3.7. Practical application

The sensor was used in chicken feed, fish, chicken and shrimp samples to evaluate its practical application. Upon addition of 100 μL sample solution into 5.0 mL 0.1 M H_2SO_4, the semi-derivative DPV curves were recorded from 0.80 to 1.15 V after 180–s accumulation at 0.6 V. There are oxidation peaks attributing to TC in chicken feed and chicken samples extract. As seen in Fig. 8, curve a, one oxidation peak at 1.07 V was observed in chicken feed sample on the sensor. After a known amount of TC standard solution was added into, the semi-derivative DPV curve was then recorded in Fig. 8, curve b. It was found that the oxidation peak current increased correspondingly after addition of TC standard. And the content of TC in chicken feed and chicken samples can be achieved according to the oxidation peak current ratio, which is shown in the second column of Table 3. However, no evident peak was observed in fish and shrimp samples. This may because no TC exists in the purchased fish and shrimp, or the concentration level of TC is lower than the detection limit of this sensor. Each sample was determined by three times, and the RSD was lower than 5% (shown in the third column of Table 3), revealing good precision. In addition, the recovery of TC standard was also performed by adding known concentration of TC standard in each sample, and the value of recovery was over the range from 97.2% to 103% (shown in the fourth, fifth and sixth columns of Table 3), indicating that this sensor has promising application.

4. Conclusion

In this work, a new sensor based on a Fe/Zn–MMT film modified glassy carbon electrode was first developed for studying the direct

electrochemical oxidation of tetracycline (TC). The super characteristics of Fe/Zn–MMT, such as large surface area, high adsorptive ability, rich active sites, subtle electronics properties and strong catalytic capacity can improve the sensitivity to detect TC. This sensor has been successfully applied to determine the concentration of TC in chicken feed, fish, chicken and shrimp samples, foreseeing its promising application as s simple, convenient, and fast electrochemical route for the determination of TC in real samples.

Acknowledgment

This research is supported by the National Nature Science Foundation of China (No. 61201091).

References

[1] J.M. Dewdney, L. Maes, J.P. Raynaud, F. Blanc, J.P. Scheid, T. Jackson, S. Lens, C. Verschueren, Food Chem. Toxicol. 29 (1991) 477–483.
[2] A.J. Alanis, Arch. Med. Res. 36 (2005) 697–705.
[3] P. Calza, S. Marchisio, C. Medana, C. Baiocchi, Anal. Bioanal. Chem. 396 (2010) 1539–1550.
[4] T. Heberer, Toxicol. Lett. 131 (2002) 5–17.
[5] R. Li, Y. Zhang, C.C. Lee, L. Liu, Y. Huang, J. Sep. Sci. 34 (2011) 1508–1516.
[6] X. Ding, S. Mou, J. Chromatogr. A 897 (2000) 205–214.
[7] Y.L. Han, Z.H.L. Zhou, R.M. Ransohoff, J. Immunol. 163 (1999) 1435–1440.
[8] J.J. Li, Y. Cao, M.R. Young, N.H. Colburn, Mol. Carcinog. 29 (2000) 159–169.
[9] M. Thaker, P. Spanogiannopoulos, G.D. Wright, Cell. Mol. Life Sci. 67 (2010) 419–431.
[10] I. Chopra, M. Roberts, Microbiol. Mol. Biol. R, 65, 232–260.
[11] X.Q. Yang, C.X. Yang, X.P. Yan, J. Chromatogr. A 1304 (2013) 28–33.
[12] K.I. Gabrovska, S.I. Ivanova, Y.L. Ivanov, T.I. Godjevargova, Anal. Lett. 46 (2013) 1537–1552.
[13] G.Y. Chen, Q.Q. Li, G.Y. Liu, F. Qin, Y. Du, Phys. Methods Food Anal. 1138 (2013) 49–63.
[14] M.B. Gholivand, H. Khani, Electroanalysis 25 (2013) 461–467.
[15] L. Zhou, D.J. Li, L. Gai, J.P. Wang, Y.B. Li, Sens. Actuators B Chem. 162 (2012) 201–208.
[16] F. Conzuelo, M. Gamella, S. Campuzano, A.J. Reviejo, J.M. Pingarrón, Anal. Chim. Acta 737 (2012) 29–36.
[17] H.T. Wang, H.M. Zhao, X. Quan, S. Chen, Electroanalysis 23 (2011) 1863–1869.
[18] C.M.F. Calixto, P. Cervini, É.T.G. Cavalheiro, J. Braz. Chem. Soc. 23 (2012) 938–943.
[19] P. Masawat, J.M. Slater, Sens. Actuators B Chem. 124 (2007) 127–132.
[20] H.T. Wang, H.M. Zhao, X. Quan, Front. Environ. Sci. Eng. 63 (2012) 313–319.
[21] G.P. Guo, F.Q. Zhao, F. Xiao, B.Z. Zeng, Int. J. Electrochem. Sci. 4 (2009) 1365–1372.
[22] X.P. Dang, C.G. Hu, Y.L. Wei, W.H. Chen, S.S. Hu, Electroanalysis 16 (2004) 1949–1955.
[23] X.J. Bo, J. Bai, J. Ju, L.P. Guo, Anal. Chim. Acta 675 (2010) 29–35.
[24] K.J. Chen, K.C. Pillai, J. Ricka, C.J. Pan, S.H. Wang, C.C. Liu, B.J. Hwang, Biosens. Bioelectron. 33 (2012) 120–127.
[25] E. Günister, D. Pestreli, C.H. Ünlü, O. Atıcı, N. Güngör, Carbohydr. Polym. 67 (2007) 358–365.
[26] G.B.B. Varadwaj, S. Rana, K. Parida, Chem. Eng. J. 215–216 (2013) 849–858.
[27] G.B.B. Varadwaj, S. Rana, K.M. Parida, Dalton Trans. 42 (2013) 5122–5129.
[28] A. Jha, A.C. Garade, M. Shirai, C.V. Rode, Appl. Clay Sci. 74 (2013) 141–146.
[29] S. Yariv, in: M.E. Schrader, G. Loeb (Eds.), Modern Approaches to Wettability: Theory and Application, Plenum Press, New York, 1992, pp. 279–326.
[30] G. Wei Wang, Q.Q. Hao, Z.T. Liu, Z.W. Liu, Appl. Catal. A Gen. 405 (2011) 45–54.
[31] A.J. David, B. Durgadas, N. Buddhadeb, J. Org. Chem. 52 (1987) 276–278.
[32] A.J. Bard, L.R. Faulkner, Electrochemical Methods Fundamentals and Applications, Wiley, New York, 1980.
[33] S. Yuan, C.G. Hu, S.S. Hu, Electrochim. Acta 51 (2006) 5274–5285.